Molecular & Biochemical Parasitology 236 (2020) 111266

Contents lists available at ScienceDirect

Molecular & Biochemical Parasitology

journal homepage: www.elsevier.com/locate/molbiopara

The recognition of proteasomal receptors by *Plasmodium falciparum* DSK2

Ishita Gupta[a,b], Sameena Khan[b,*]

[a] Structural Immunology Group, International Centre for Genetic Engineering and Biotechnology, New Delhi, Delhi, India
[b] Drug Discovery Research Centre, Translational Health Science and Technology Institute, NCR Biotech Science Cluster, 3rd Milestone, Gurgaon-Faridabad Expressway, Faridabad, Haryana, 121001, India

ARTICLE INFO

Keywords:
Shuttle factors
Proteasome receptors
Ubiquitin
Ubiquitin-like domain
Plasmodium falciparum
Surface plasmon resonance

ABSTRACT

One of the pathways by which proteins are targeted for degradation by the proteasome involve transport by shuttle proteins to proteasomal receptors. The malaria parasite *Plasmodium falciparum* has recently been found to possess a similar pathway, with the shuttle protein PfDsk2 being the major player. In this study, we have demonstrated how PfDsk2 and its recognition by proteasomal receptors differ from the mammalian system. Our crystal structure of unbound PfDsk2 UBL domain at 1.30 Å revealed an additional 3_{10}-helix compared to the human homolog, as well as a few significant differences in its putative binding interface with the proteasome receptors, PfRpn10 and PfRpn13. Moreover, the non-binding face of UBL showed a reversal of surface charge compared to HsDsk2 shuttle protein, instead resembling HOIL-like E3 ligase UBL domain. The affinity of the interaction with the proteasomal receptors remained similar to the human system, and dissociation constants of the same order of magnitude. On the other hand, we have found evidence of a novel interaction between $PfRpn13^{DEUBAD}$ with the $PfDsk2^{UBL}$ suggesting that PfDsk2 may work in cooperation with deubiquitinating enzymes for proofreading ubiquitinated substrates. Our study provides the first molecular look at shuttle proteins in Apicomplexan parasites and hints at how their interaction landscape might be broader than what we may expect.

1. Introduction

Shuttle proteins target proteins for degradation to the proteasome via interacting with proteasome receptors [1,2]. In *Plasmodium*, protein degradation is crucial for high replication rate, rapid progression of a complex life cycle in human host and mosquito vector and accumulation of thermal stress proteins in the host [3,4]. In eukaryotes, a similar regulation of protein degradation is essential to maintain cellular homeostasis [5,6]. Shuttle proteins are known to facilitate the timely degradation of mislocalized mitochondria membrane proteins and transmembrane domain proteins [7,8]. One of the first identified shuttle proteins in parasites, Dsk2, has been shown to interact with early transmembrane protein 5 (ETRAMP-5) by using yeast two hybrid screens [9]. The ETRAMP proteins are essential for parasite blood stage virulence, theorized to be the major protein component of the parasitophorous vacuolar membrane [10,11]. However, the nature of plasmodial shuttle proteins themselves, their interaction with the parasite proteasome as well as their role in regulating crucial virulence factors is still unknown.

Drawing from our existing knowledge in humans and yeast, shuttle proteins are known to interact with proteasome receptors for the degradation of ubiquitin-tagged proteins. Shuttle proteins such as Dsk2 are composed of ubiquitin-like and ubiquitin-associated domains (UBL-UBA) at the N and C-termini, respectively [12]. The STI (Stress Induced Phosphoprotein) domain present in the middle is responsible for binding to chaperone proteins and assist in degradation of misfolded proteins [13]. Dsk2 works in association with the proteasome receptors Rpn10/S5a, Rpn13/Adrm1 and Rpn1, with its UBL domain being the main player mediating recognition [14–16] and the UBA domain responsible to interact with the ubiquitinated substrate protein [22].

Shuttle proteins play roles in cell cycle control, spindle body duplication and DNA repair [17–19]. The functions of these proteins have been well characterized in humans and *Saccharomyces cerevisiae* [19–23]. Among Apicomplexans, shuttle proteins have been putatively identified by a computational approach, in *Plasmodium falciparum* [24]. In *Drosophila,* Dsk2 protein deletion is known to cause impaired

Abbreviations: UBL, ubiquitin-like domains; UBA, ubiquitin-associated domains; UIMs, ubiquitin-interacting motifs; STI, stress induced phosphoprotein; Pru, pleckstrin-like receptor; SPR, surface plasmon resonance; TLS, translation/libration/screw; NHS, *N*-hydroxysuccinimide; EDC, ethyl(dimethylaminopropyl) carbodiimide

* Corresponding author.
E-mail address: sameena@thsti.res.in (S. Khan).

https://doi.org/10.1016/j.molbiopara.2020.111266
Received 14 December 2019; Received in revised form 7 February 2020; Accepted 8 February 2020
Available online 11 February 2020

proteolysis while in yeast, accumulation of ubiquitinated proteins occurs [25–27]. In humans, Dsk2 is referred to as UBQLN (Ubiquilin) and is responsible for targeting aggregation-prone and mislocalized membrane proteins to the proteasome, protecting cells from stress and damage [7,13,28]. The above points broadly indicate the importance of Dsk2 in the maintenance of cellular homeostasis and also indirectly in the control of parasite pathogenicity by regulating the turnover of virulence proteins such as ETRAMP-5. Prior to understanding specific substrate recognition mechanisms, we have attempted to delineate the general mechanism by which plasmodial shuttle proteins recognize proteasomal receptors as well as the structural features of the shuttle proteins that allow recognition, using our existing knowledge in the human system as a reference.

Here, our crystal structure of the unbound form of N-terminal UBL domain of PfDsk2 at 1.30 Å shows how Dsk2 differs from the human ortholog and how these differences affect the affinity of its interaction with corresponding domains of proteasome receptors PfRpn10 and PfRpn13. We have further tested the universality of these differences in PfRad23, a second shuttle protein identified in *P. falciparum*, by sequence comparisons and affinity measurements.

2. Materials and methods

2.1. Construction of plasmids

Codon optimized cDNA for *E. coli* expression of PfDsk2, PfRad23, PfRpn13, and PfRpn10 were obtained from GeneArt. Different domains of the above clones were amplified by polymerase chain reaction and subcloned into a pETM11 vector, downstream of a TEV protease-cleavable N-terminal 6xHis-tag for *E. coli* expression. Primers used for amplification are listed in Supplementary Table 1. The clonings were confirmed by DNA sequencing (Macrogen).

2.2. Protein expression and purification

E. coli B834 cells were transformed with the expression vector and grown in LB medium containing 50 µg/ml kanamycin. Protein expression was induced at OD_{600} of 0.8 with 0.5 mM IPTG and cells were collected after 18 h incubation at 18 °C. Cells were lysed by sonication in lysis buffer (50 mM Tris-HCL pH 8.0, 300 mM NaCl, 15 mM imidazole and 5 mm β-mercaptoethanol) in the presence of protease inhibitor. The proteins were purified by affinity chromatography using Ni-NTA beads (Qiagen) and eluted with 100 mM or 250 mM imidazole buffer. The His tag of the proteins was cleaved with His-tagged TEV protease at 16 °C overnight followed by dialysis into 50 mM Tris-HCL pH 7.0 buffer, containing 300 mM NaCl and 15 mM imidazole for 18 − 20 h at 4 °C. The His-tagged TEV protease was subsequently removed by nickel affinity chromatography. Proteins were concentrated using Amicon centrifugal filters (3 kDa MWCO, Millipore) and loaded onto a Superdex 75 10/300 G L column (GE Healthcare) equilibrated with 10 mM Hepes pH 7.5 buffer, containing 150 mM NaCl and 1 mM DTT, after which the positive fractions were concentrated. For purification of $PfRpn13^{Pru}$ (1–141) and $PfRpn13^{DEUBAD}$ (143–253), $PfRpn10^{UIM2}$ (227–296), an additional step of anion exchange using HiTrap Q HP column (GE Healthcare) was carried out before loading to Superdex 75 10/300 G L column. The His-tagged proteins for surface plasmon resonance studies were purified using nickel affinity, anion exchange and size-exclusion chromatography.

2.3. Protein crystallization and Data collection

Crystals were grown by vapor diffusion in hanging drops at 20 °C. $PfDsk2^{UBL}$ at a concentration of 6 mg/ml was mixed with an equal volume of reservoir solution containing 0.1 M Bis-Tris pH 6.5 and 2 M ammonium sulfate. Crystals suitable for X-ray diffraction appeared within 24 − 48 h. Crystals were mounted and cryocooled in liquid nitrogen. Data were collected at a resolution of 1.30 Å on the ID23-1 beamline at European Synchrotron Radiation Facility [29–31].

Table 1
X-ray data collection and refinement statistics. Values in parenthesis are for the highest resolution shell.

PDB ID	6JL3
Data collection	
Wavelength (Å)	0.968622
Resolution Range (Å) (outermost shell)	35.46–1.303 (1.35–1.303)
Space Group	P 41 21 2
Unit cell Parameters	
a, b, c (Å)	70.927 70.927 28.122
α = β = γ (°)	90
Total Reflections	146637 (12428)
Unique Reflections	18009 (1711)
Completeness (%)	99.45 (95.89)
Average I/sigma(I)	24.47 (2.65)
Multiplicity	8.1 (7.3)
R merge	0.04347 (0.6308)
R pim	0.01616 (0.2466)
CC1/2	0.999 (0.934)
Refinement	
Reflections used in Refinement	17994 (1701)
Reflections used for R free	1799 (170)
R work	0.156
R free	0.168
Protein residues	74
No. of non-hydrogen atom	667
RMS deviation	
Bond Length (Å)	0.005
Bond Angles (°)	0.838
Ramachandran plot (%)	
Most favoured	98.61
Allowed	1.39
Outliers	0
	16.26

2.4. Structure solution and refinement

Diffracted data collected on the $PfDsk2^{UBL}$ crystal was processed with XDS and scaled with Aimless from the CCP4 suite [32,33]. The structure was solved by molecular replacement with Phaser-MR (Phenix) using the 1.15 Å resolution structure of $Dsk2^{UBL}$ domain of *Saccharomyces cerevisiae* (PDB ID-2BWF) [34,35]. Model building and refinement of the structure was performed through rounds of refinement using Coot and Phenix-Refine [36,37]. Translation/libration/screw (TLS) parameters generated from the TLSMD server were used during the refinement. Water molecules were added at the end of refinement. The final R_{work} and R_{free} values were 0.156 and 0.168, respectively. The crystal data and structure refinement parameters are listed in Table 1. The atomic coordinates and structure factors have been deposited in Protein Data Bank with accession code 6JL3. All the structures were analyzed and their images generated using Chimera 1.11.2 and Pymol v2.x [38,39]. Surface electrostatics were computed using APBS after protonating with the Amber forcefield at a simulated pH of 7.0. Interface analysis of $HsDsk2^{UBL}$ complex with $HsRpn13^{Pru}$ was performed using PDBe PISA web server [40].

2.5. Homology modeling

$PfRpn13^{Pru}$ sequence was obtained from UniProt database (ID: Q8ILV5), and was subjected to the BLASTp search to find a suitable template from Protein Data Bank. The protein template retrieved was Human Rpn13 structure (PDB ID-2NBV, UniProt ID: Q16186) with sequence identity of 33.6 % and submitted to the SWISS-MODEL homology modelling server [41], to obtain a three-dimensional model of $PfRpn13^{Pru}$. Further, PSVS was used to validate the stereochemistry of the modeled structure [42].

2.6. Surface plasmon resonance binding

Surface Plasmon Resonance experiments were carried out on a Biacore T200 instrument (GE Healthcare) at 25 °C. The binding experiments were performed in buffer HBS-P + buffer (10 mM HEPES pH 7.4, 150 mM NaCl, and 0.005 % P20). The flow system was primed with the running buffer before the initiation of the experiment. Different coupling methods were optimized on different sensor surfaces for each interaction, as the proteins showed non-specific binding to the reference surface due to their hydrophobic nature. $PfDsk2^{UBL}$ and $PfRad23^{UBL}$ were captured on an NTA sensor chip (GE Healthcare) via its His-tag to an immobilization level of approximately 1500 RU. The binding experiments were carried out in a single cycle kinetics mode. $PfRpn13^{Pru}$ was serially diluted in running buffer, and injected at a flow rate of 30 µl/min across both surfaces for 120 s, while dissociation was set up for 60 s. $PfRpn13^{DEUBAD}$ was serially diluted in running buffer, and injected at a flow rate of 30 µl/min across both surface for 60 s, with dissociation for 60 s. $PfRpn10^{UIM2}$ (238–283) was directly immobilized on a CM5 sensor chip (GE Healthcare) by standard amine coupling chemistry using N-hydroxysuccinimide (NHS) and ethyl(dimethylaminopropyl) carbodiimide (EDC), to an immobilization level of approximately 1500 RU on Fc2. Unreacted NHS-esters were blocked by ethanolamine HCl. $PfDsk2^{UBL}$ and $PfRad23^{UBL}$ were serially diluted in running buffer, and injected at a flow rate of 30 µl/min across both surface for 60 s and dissociation were set up for 60 s. The analysis was done using Biaevaluation (GE Healthcare) and GraphPad Prism 7 software (GraphPad Software Inc, USA). The reference flow cell was left unmodified and the data from the reference flow cell were subtracted for all runs. The equilibrium dissociation constants (K_D) were determined by plotting the measured response (R_{eq}) as a function of the analyte concentration. The data was further fitted to a 1:1 binding model of nonlinear regression (specific binding) using Graph Pad Prism [43,44]. The experiments were performed in duplicates.

3. Results

Prior to determining the mechanism underlying recognition of proteasomal receptors by the UBL domain of PfDsk2, a pairwise sequence alignment performed using ESPript software [45] provided valuable information regarding the domain architecture of PfDsk2 and how its sequence differs from the human ortholog. The sequence alignment analysis reveals HsDsk2 to be double length (624 residues) compared to PfDsk2 (388 residues) (Fig. 1A and B). PfDsk2 possesses a UBL domain at the N-terminus, connected by a short linker to the STI domain, followed by the UBA domain at the C-terminus (Fig. 1A). The UBL domain was found to possess two major binding sites for proteasomal receptors that are mostly conserved (Fig. 1C), barring a few divergent residues such as Lys50, Asp69, Met71, Arg75 and Ser76. Moreover, loops and secondary structures surmised to be a part of the interface with proteasomal receptors were also found to possess a few differences. These indicated a partial divergence in the structural features of the UBL domain, which would ultimately affect the recognition of proteasomal receptors. Another distinct feature is absence of 30 amino acid residues at the N-terminus in PfDsk2 before the presence of the UBL domain which is prominently present in HsDsk2. While unrelated to proteasomal recognition, it was also interesting to note that there was just a single STI domain in *P. falciparum* compared to four in humans (Fig. 1A and B). Other variations could also be seen within the linker region between the two domains (UBL and STI), which is shorter by 74 amino acids in *P. falciparum* (Fig. 1A and B).

Interestingly, PfDsk2 crucial domain UBL responsible to mediate interaction with proteasome receptor shows sequence similarity about 33.8 % with human homolog suggesting it to share similar conserved function such as regulating intracellular protein degradation, thereby affecting diverse cellular functions, including removing misfolded and regulatory proteins. Comparison of UBL as well as full-length Dsk2 among the different species of *Plasmodium* highlighted the sequence conservation in the domains across the plasmodia, with the only observable difference being the linkers connecting the domains (Supplementary Fig. S1A).

3.1. Crystal structure of Dsk2-UBL reveals a conserved Ub β-grasp fold

Sequence differences with the human UBL domain indicated changes in surface chemistry and space-filling properties of $PfDsk2^{UBL}$. To have a better understanding of the binding site of the UBL domain of Dsk2, we have crystallized $Dsk2^{UBL}$ in the apo form and collected high-resolution X-ray diffraction data at 1.30 Å resolution (Supplementary Fig. S2A and B). The crystals belonged to space group P4212, with one molecule in the asymmetric unit and a solvent content of 39.68 %. The crystal structure revealed that the $PfDsk2^{UBL}$ has a compact ubiquitin β-grasp fold (Fig. 2A) with a five stranded β-sheet and one α-helix of 3.5 turns placed perpendicular to it and two 3_{10}-helices. The first and last β-strand are oriented parallel to each other and other β-strands are antiparallel to each other.

Secondary structural elements and hydrophobic residues are listed in Supplementary Table S2. The electron densities of two additional amino acids Met1 and Ala2 from the tag at N terminus and last three amino acids Ala77, Met78, Ala79 at C terminus was missing from the structure and are excluded. A composite omit map was calculated using the Phenix autobuild program with simulated annealing showing a well-defined electron density of the binding sites (Supplementary Fig. S2C, D and E).

3.2. Structural differences of PfDsk2 UBL with human Dsk2 UBL

The structure of human and *Plasmodium* UBL domain of Dsk2 superimposed with a root mean square deviation of 1.93 Å over 73 aligned Cα positions (Fig. 2B). For comparison with human Dsk2 UBL ($HsDsk2^{UBL}$), model 4, the centroid structure of the NMR ensemble (PDB ID-1J8C) was used for comparison [16]. The deviations of Cα atom per residue upon superimposition of these structures is provided (Supplementary Fig. S2F), which indicated that the backbone of Dsk2 UBL domain of *Plasmodium* is organized into a ubiquitin-like β grasp fold similar to the human counterpart, with the slight tilt of α helix, deviation of the β3 strand and the loop regions in PfDsk2 compared to HsDsk2 (Fig. 2B).

The first core binding surface is made out of β3, β3-β4 loop and β4 of $HsDsk2^{UBL}$ formed by amino acids Ile75, Phe76, Ala77, Gly78, Lys79, Ile80 and Leu81 (Fig. 3B), corresponding to Ile48, Phe49, Lys50, Gly51, Lys52, Ile53 and Leu54 in $PfDsk2^{UBL}$ (Fig. 3A) [40–42]. The second contact surface is on the β5 of $HsDsk2^{UBL}$ formed by amino acids Leu96, Thr97, Val98, His99 and, Val101 (Fig. 3B), corresponding to Asp69, Thr70, Met71, His72 and Val74 in $PfDsk2^{UBL}$ (Fig. 3A). These residues form the binding site for interaction with the proteasome receptors, with a total binding area of 718 $Å^2$ in $PfDsk2^{UBL}$ (Fig. 3A). The amino acids on the binding surface of $PfDsk2^{UBL}$ form a similar mixed hydrophobic/charged surface as of $HsDsk2^{UBL}$ for mediating the interaction with the proteasome receptors (Fig. 3C and D). The surface electrostatics of the proteasome receptor binding site on the $PfDsk2^{UBL}$ also indicated a partially positively charged binding surface, similar to that seen for $HsDsk2^{UBL}$ (Fig. 3E and F). This similarity in binding surface might also imply it has similar substrate proteins such as cell cycle regulators which would affect parasite life cycle. This influence on parasite life cycle would further govern survival and pathogenicity of parasite which could be further confirmed by identification of substrate protein partners.

A distinct feature was observed when the surface electrostatic potential of the α-helix from both $PfDsk2^{UBL}$ and $HsDsk2^{UBL}$ was compared. The solvent exposed surface of the α-helix is formed by acidic residues in $PfDsk2^{UBL}$, creating a net negative surface charge (Fig. 4A). The same region is composed of basic residues in $HsDsk2^{UBL}$ (Fig. 4B),

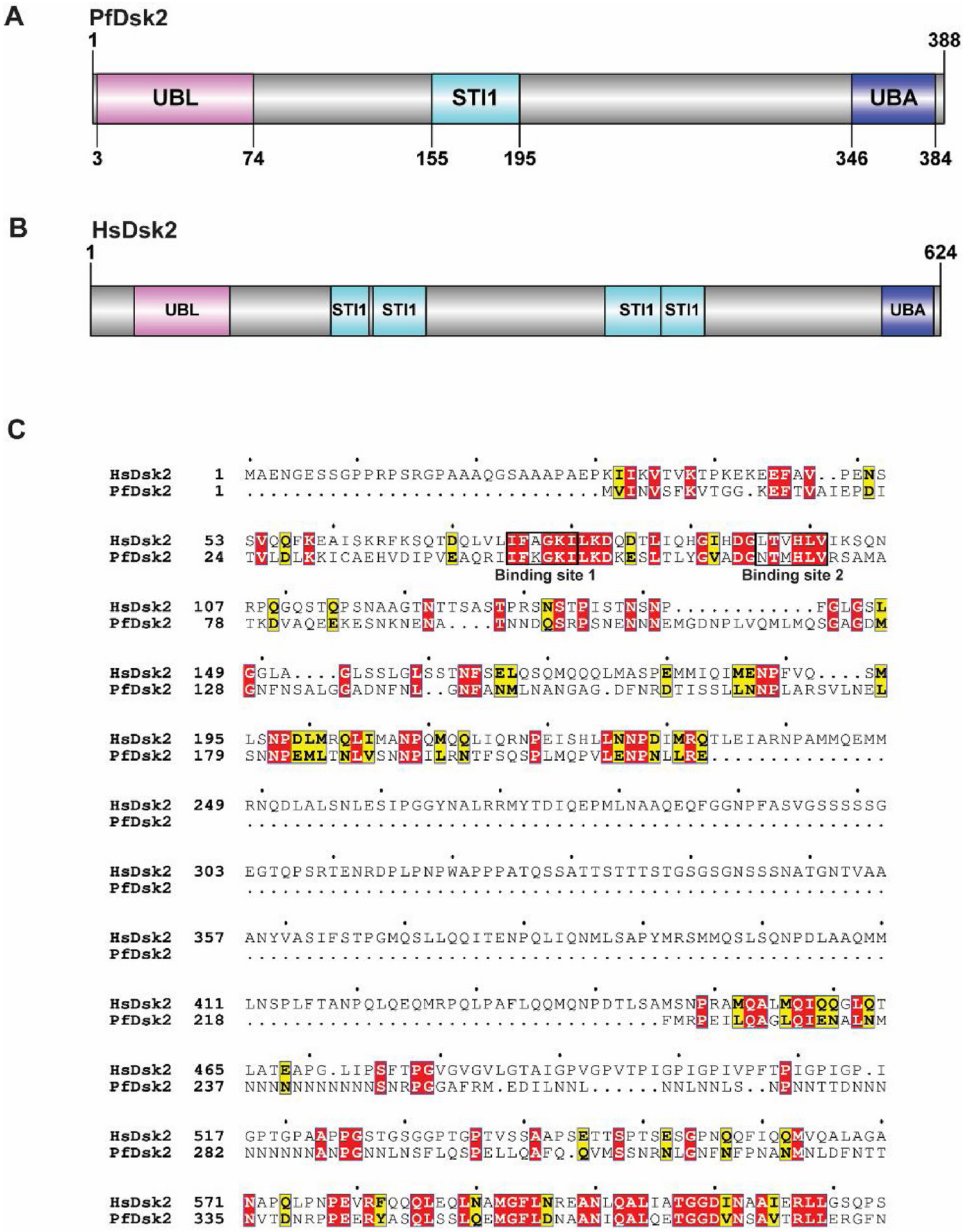

Fig. 1. Sequence analysis of *Plasmodium falciparum* Dsk2 (PfDsk2) protein. (A) Domain architecture of PfDsk2, showing the UBL, STI1 and UBA domain. The UBL domain construct is used in the study. (B) Domain architecture of HsDsk2 protein, showing UBL, STI1 and UBA domain. (C) ClustalW sequence alignment of PfDsk2 with Human Dsk2 (HsDsk2). The N-terminal stretch of 28 residues is absent in *Plasmodium*. The numbering at the top corresponds to the amino acid numbers of HsDsk2. Two boxed regions in black correspond to the binding site present in Dsk2 for binding to proteasome receptors.

creating a net positive charge. Most notably, Asp39 and Glu36 in PfDsk2^{UBL} are located where Lys63 and Lys66 are in HsDsk2 ^{UBL}, resulting in an opposite electrostatic potential. The α- helix is not involved in the interaction with the proteasome receptors, but in other UBLs such as HOIL E3 ligase, the role is well illustrated [47]. Comparing surface electrostatics of the HOIL^{UBL} (Fig. 4C) α- helix with PfDsk2^{UBL} showed similar charge distribution (Fig. 4A). This holds the possibility of unique interactions of PfDsk2^{UBL} with additional partners in *Plasmodium*. Comparing with known interfacial amino acids of HOIL^{UBL}, Lys32 and Glu36 on the solvent exposed surface of PfDsk2^{UBL} could aid the interaction with such binding partners (Fig. 4D).

3.3. Comparison of modeled PfRpn13 Pru domain with HsRpn13 Pru domain

Rpn13 is the proteasome receptor protein and one of its domain Pru is involved in interaction with the UBL domain of Dsk2. A preliminary model of the Pru domain of PfRpn13 was calculated by using the HsRpn13 structure as a template in the SWISS-MODEL server. The summary of structure factors for validation of model is listed in Supplementary Table S3. The model was used to confirm whether a complementary, negative surface on the proteasomal receptor is present for interaction with the Dsk2 protein. HsRpn13^{Pru} (PDB ID:5IRS) was found to have a negative binding surface for interaction with the HsDsk2^{UBL} (Fig. 5B), however PfRpn13^{Pru} showed a less negative binding surface (Fig. 4A), indicating that electrostatic interactions possibly do not dominate binding process in PfDsk2^{UBL}. Hydrophobic surface comparison of HsRpn13^{Pru} and PfRpn13^{Pru} showed HsRpn13^{Pru} (Fig. 5D) to be more hydrophobic than PfRpn13^{Pru} (Fig. 5C). As seen in the structure of HsDsk2^{UBL} and HsRpn13^{Pru} complex, hydrophobic and electrostatic interactions play a major role and these interactions seem to be weakened in *Plasmodium*.

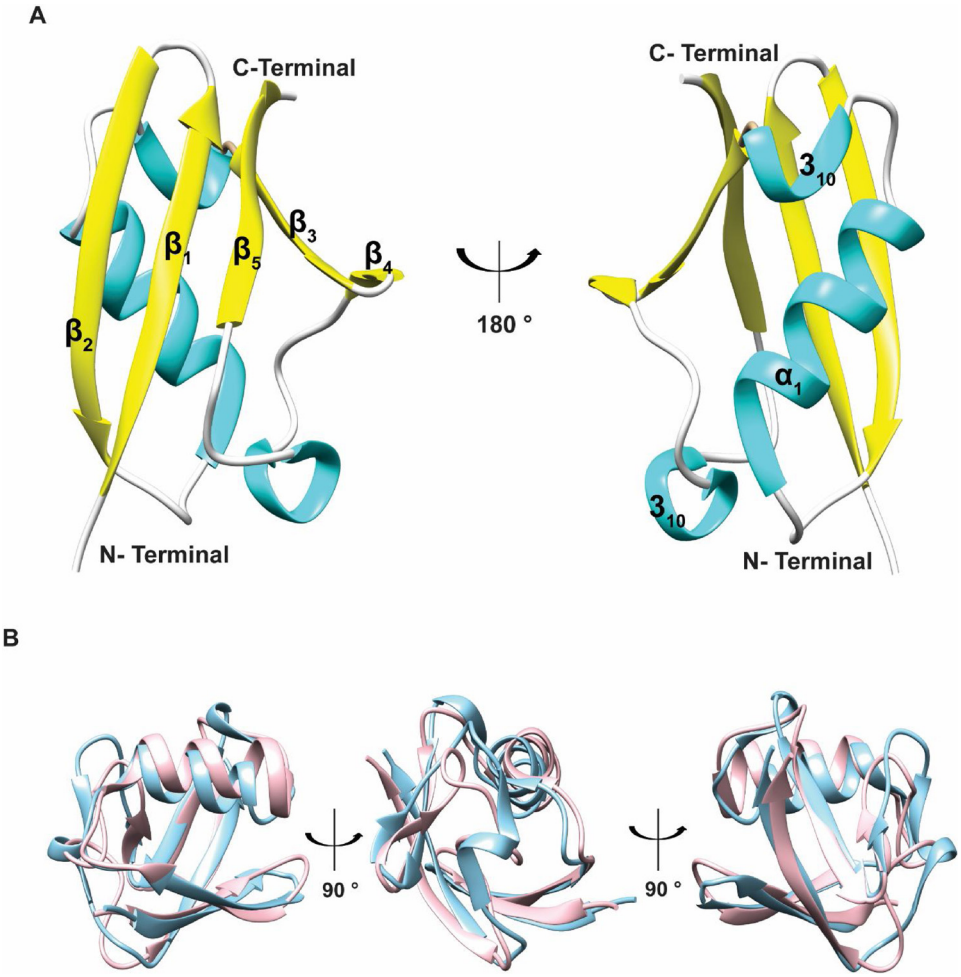

Fig. 2. Crystal structure of PfDsk2^{UBL} and structural comparison with HsDsk2^{UBL}. (A) Crystal structure of PfDsk2^{UBL} showing the ubiquitin β-grasp fold (PDB ID-6JL3). Secondary structure elements are labelled. (B) Ribbon representation of the overlay of PfDsk2^{UBL} (sky blue) with HsDsk2^{UBL} (pink).

Despite the similarity of the two contact surfaces there are some noteworthy changes to be highlighted. One of them is the substitution of Ala77 with Lys50 at the first binding surface in PfDsk2^{UBL}. Interestingly, Ala77 forms a hydrogen bond with Lys103 of HsRpn13^{Pru} (Fig. 3F). Its substitution with Lys50 in PfDsk2^{UBL} (Fig. 3E), creates a positive surface on the β3-β4 loop which would potentially alter the interaction with PfRpn13^{Pru} [48]. A sequence comparison between PfRpn13 and HsRpn13 was carried out to determine whether there was any corresponding substitution on the receptor. Notably, in the PfRpn13^{Pru} domain, Lys103 was substituted by Glu86 indicating that the mode of interaction for the UBL β3-β4 loop with PfRpn10 was possibly altered from hydrogen bonding to salt bridges, providing a long-range, stronger binding (Supplementary Fig. S3A).

The analysis of the complex of HsDsk2 ^{UBL} with HsRpn13^{Pru} (PDBID-2NBV) shows amino acid residues Leu96 and Val98 on the second binding site participate as the interfacing residues while mediating interaction with the HsRpn13^{Pru}. These residues are substituted with Asn69 and Met71 respectively in PfDsk2^{UBL}. These changes were reflected in a more favorable hydrophobic surface in HsDsk2^{UBL} (Fig. 3D) compared to PfDsk2^{UBL} (Fig. 3C).

Another crucial residue is His99 in HsDsk2^{UBL} which is observed to be conserved across species for Dsk2 and also in ubiquitin (Supplementary Fig. S3B). His99 in HsDsk2^{UBL} is responsible for hydrogen bond interaction with Asp78 and Asp79 of proteasome HsRpn13^{Pru}. In PfDsk2^{UBL} it is conserved as His72. The corresponding amino acids on PfRpn13^{Pru} are Lys61 and Ser62. This substitution of amino acid resulted in a striking change in surface electrostatic potential, with a change of negative charge in the HsRpn13^{Pru} (Fig. 5B) to a positive charge in the modeled PfRpn13^{Pru} (Fig. 5A). While hydrogen bonding between histidine and lysine is not uncommon, the interaction would possibly be weaker owing to the electrostatic repulsion.

The positions of amino acids Lys79 and Ile80 in HsDsk2^{UBL} are crucial as they are responsible to form the core contact surface and also bring the β4 strand near the HsRpn13^{Pru} for additional hydrogen bonding [48]. Structural comparison of the same residues in PfDsk2^{UBL} shows a slight change in the side chain orientations of Lys52 and Ile53. Given that NMR ensembles often show several side-chain orientations, we confirmed the difference against all models (data not shown), while displaying the comparison with model 4 only, for clarity (Fig. 5E and F). Lys79 mediates hydrogen bonding with Asp72 of HsRpn13^{Pru}. PfRpn13^{Pru} shows Asn56 at a similar position with Asp55 as its neighbor, which could possibly interact with Lys52 of PfDsk2^{UBL}. The shift in side chain of Lys52 could confer the ability of the PfDsk2^{UBL} to form similar core contacts but with a slightly distant amino acid (Asp55) in the PfRpn13^{Pru}.

The above-mentioned detail analysis of the published complex structure of HsRpn13^{Pru} with HsDsk2^{UBL} in comparison with modeled structure of PfRpn13^{Pru}, highlights some similar and some distinct residues which influence the affinity of interactions and the preference to different proteasome receptors due to redundant role. An experimentally determined structure of the complex could help to further validate this possibility.

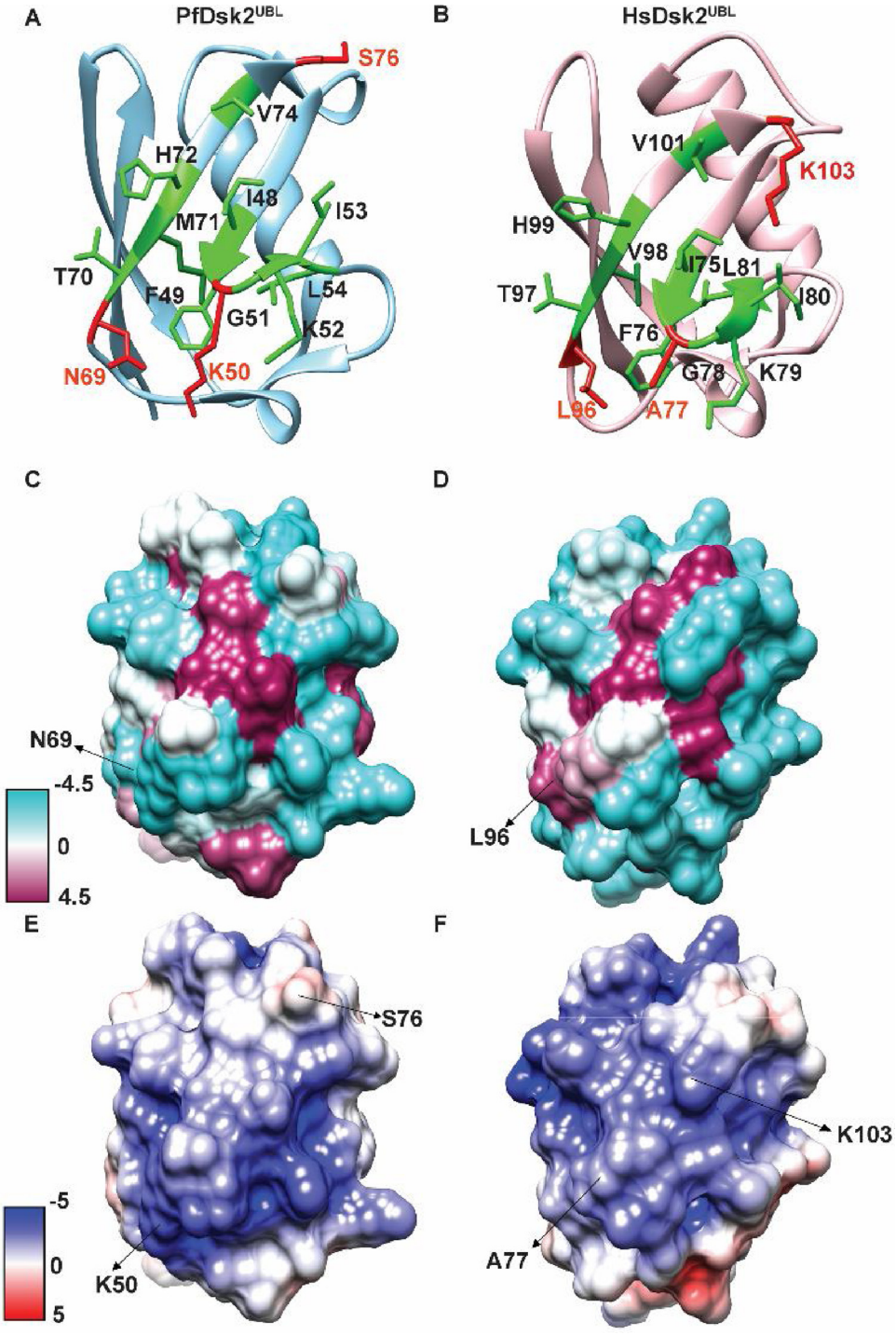

Fig. 3. Comparison between (A) PfDsk2 ^{UBL} (B) HsDsk2^{UBL}. Residues identical are highlighted in green and similar are highlighted in dark green. Residues which are different are highlighted and labeled in red. (C) Hydrophobic surface representation of PfDsk2^{UBL} and (D) HsDsk2^{UBL} hydrophobic surface is represented by using the Kyle-Doolittle scale in the range of −4.5 to +4.5, with cyan for most hydrophilic to maroon for most hydrophobic residues. The interfacial residue on second binding site of the Dsk2 UBL domain for interaction with proteasome receptor (Rpn13^{Pru}) is Leu96 on HsDsk2 ^{UBL} and is substituted with Asn69 on PfDsk2^{UBL}. (E) APBS-derived surface electrostatics of PfDsk2^{UBL} and (F) HsDsk2^{UBL} with locations of two binding-site residues highlighted. The binding site is a positive surface formed by the β3 strand, β3- β4 loop, β4 and β5 strand. The color scale is in units of kT/e ranging from −5 (red) to +5 (blue).

3.4. Comparison of binding surface formed on Dsk2 for interaction with another proteasome receptor Rpn10 UIMs domain

Similar conserved residues in the Dsk2^{UBL} mediate the interaction with the UIM domain of the other proteasome receptor, Rpn10. However, Lys103 on β5 of HsDsk2^{UBL} (Fig. 3B), which forms salt bridges with Asp213 and Glu283 of UIM1 and UIM2 respectively, is replaced with Ser76 (Fig. 3A) [46]. Sequence alignment reveals the presence of Asp202 and Asn261 in UIM1 and UIM2 respectively in plasmodia but the subsequent lysine to form salt bridges is absent, pointing towards the possibility of weaker interaction with the UIMs (Supplementary Fig. S3D and E). This is corroborated by the completely opposite surface electrostatic surface of PfDsk2^{UBL} (negative) as compared to HsDsk2^{UBL} (positive) (Fig. 3E and F).

3.5. Rpn13 domains Pru and Deubad show binding with PfDsk2^{UBL}

Dsk2 is shown to work in cooperation with the proteasome receptor Rpn13 to target proteins for degradation. Rpn13 comprises of an N-terminal Pru domain and a C-terminal Deubad domain. The Pru domain in humans plays a role to interact with the UBL domain of Dsk2 while the Deubad domain interacts with the deubiquitinating enzyme UCHL5 associated with the proteasome [48,49,51]. To interrogate the same interaction in Plasmodium, surface plasmon resonance was performed.

PfDsk2^{UBL} was captured on the NTA chip and Pru domain flowed over the chip at different concentrations. Interactions between the Pru

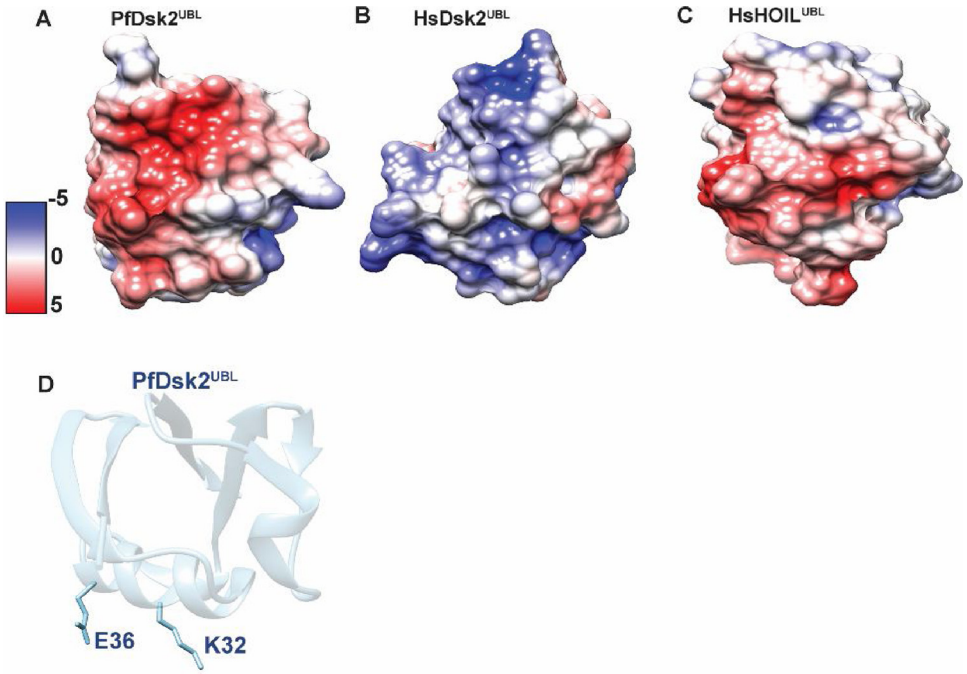

Fig. 4. APBS-derived surface electrostatics of α-helix region of (A) PfDsk2^{UBL} (B) HsDsk2^{UBL} (C) HsHOIL^{UBL} (PDB ID-2LGY). (D) Solvent exposed residues Lys32 and Glu36 present on α-helix of PfDsk2^{UBL}.

domain and UBL of PfDsk2 could be clearly seen from the binding profile at different concentration (Fig. 6A, Supplementary Fig. 4A). We observed that the Pru domain of Rpn13 shows a binding affinity (K_D) of more than 50 μM with Dsk2. Unfortunately, exact value of K_D was not being determined due to non-specific binding of protein at higher concentration on reference surface resulting in negative binding. This result correlates well with the affinity observed for UBL interactions in other systems, where the weak affinity allows for transient and readily reversible interactions. Our data is within the same order of magnitude, comparatively weaker, as that for humans as shown by NMR studies, wherein the Pru domain interacts with 9.3 μM affinity to HsDsk2 [48]. To ascertain whether a similar binding affinity is observed across all shuttle proteins in plasmodia, we also obtained dissociation constants for the interaction of another shuttle protein Rad23, with Pru. In this case also, the binding was found to occur in a similar order of magnitude, with a K_D of 42.8 μM (Supplementary Fig. S4D and E).

The C-terminal Deubad domain of Rpn13, on the other hand, has no report of interaction with shuttle proteins, instead providing a binding platform for the UCHL5 deubiquitinating enzyme. As the UCHL5 ortholog is absent in plasmodium, it is likely to bind to another deubiqutinating enzyme or play moonlighting roles. The structure of PfDsk2^{UBL} and its marginally weaker binding affinity to Pru domain indicated that the reaction between PfDsk2 and Rpn13 was overall bound to be weaker than the human ortholog. In such a case, it would be possible that PfDsk2 would form contacts with other sections of Rpn13, to ensure a similar affinity to the mammalian system. We proposed to study its interaction with the Deubad domain of PfRpn13. Surprisingly, the Deubad domain showed a positive interaction with a binding affinity (K_D) of 18.7 μM with PfDsk2^{UBL} (Fig. 6B, Supplementary Fig. 4B). This prompted us to look at the sequence of PfRpn13^{DEUBAD} to check for apparent differences with the human counterpart. The sequence alignment of the Deubad domain of the plasmodium and humans features the presence of conserved and non-conserved residues (Supplementary Fig. S3C). Some of the core helix residues responsible for interaction with UCHL5 are conserved, implying potential interaction with other deubiquitinating enzymes in plasmodia that are still not identified.

3.6. Interaction of PfDsk2^{UBL} with the UIM motifs of PfRpn10

The UIM motifs in the Rpn10 proteasome receptor are defined by the consensus sequence L/I-XX-A-φ-XX-S, where X can be any amino acid and φ is a hydrophobic residue [49]. These motifs are present as LALALRVS in UIM1 and IAYAMQMS in UIM2 in HsRpn10 and are replaced by similar consensus sequences LLNAMQLS in UIM1 and LKEALILS in UIM2 in PfRpn10 as seen in sequence alignment (Supplementary Fig. S3D and E). Prior literature related to proteasome receptor interaction with the UBL domain of HsDsk2^{UBL} has revealed the role of Leu216, Ala219, Leu220 and Ser223 in UIM1 and Ile287, Ala290, Met291 and Ser294 in UIM2 in binding to UBL [49]. Similarly, the core motifs for providing a hydrophobic interaction with PfDsk2^{UBL} have been conserved in PfRpn10 UIM1 as Leu205, Ala208, Met209, and Ser212 and as Leu263, Ala266, Leu267, Ser270 in UIM2. However, it was interesting to note the substitution of Tyr289 with Glu265 in plasmodial UIM2. Tyr289 in human UIM2 provides a more compact binding when interacting with ubiquitin and another shuttle protein Rad23 [49,53]. It was observed to form a van der Waal's interaction with leucine residues in both ubiquitin (Leu8) and Rad23 (Leu10) [53]. The replacement of Tyr289 with the Glu265 shows the possible absence of such compact interaction with ubiquitin. Similarly, other divergent substitutions such as Ala288 to Lys264, as well as Gln292 to Ile268 prompted us to check whether the interaction between UBL and UIM2 was affected in terms of affinity, in *Plasmodium*.

For studying the interaction of Rpn10 UIM2 domain with Dsk2^{UBL}, UIM2 was covalently coupled by amine coupling on CM5 chip and Dsk2 UBL was injected over the sensor chip surface. Dsk2 UBL domain was found to interact with a dissociation constant of 20.1 μM (Fig. 6C, Supplementary Fig. 4C). Compared to the human ortholog, this interaction was found to be within the same order of magnitude, with HsDsk2^{UBL} interacting with UIM2 with a binding affinity of 24.8 μM. A similar order of magnitude was also observed for Rad23, with a K_D value of more than 100 μM (Supplementary Fig. S4F and G).

Despite multiple attempts, we were not able to purify UIM1 in sufficient quantity to do SPR binding experiments. We attempted to purify with GST-tag UIM1 and subsequently used it for binding experiments, but the UBL domains showed non-specific binding to GST-

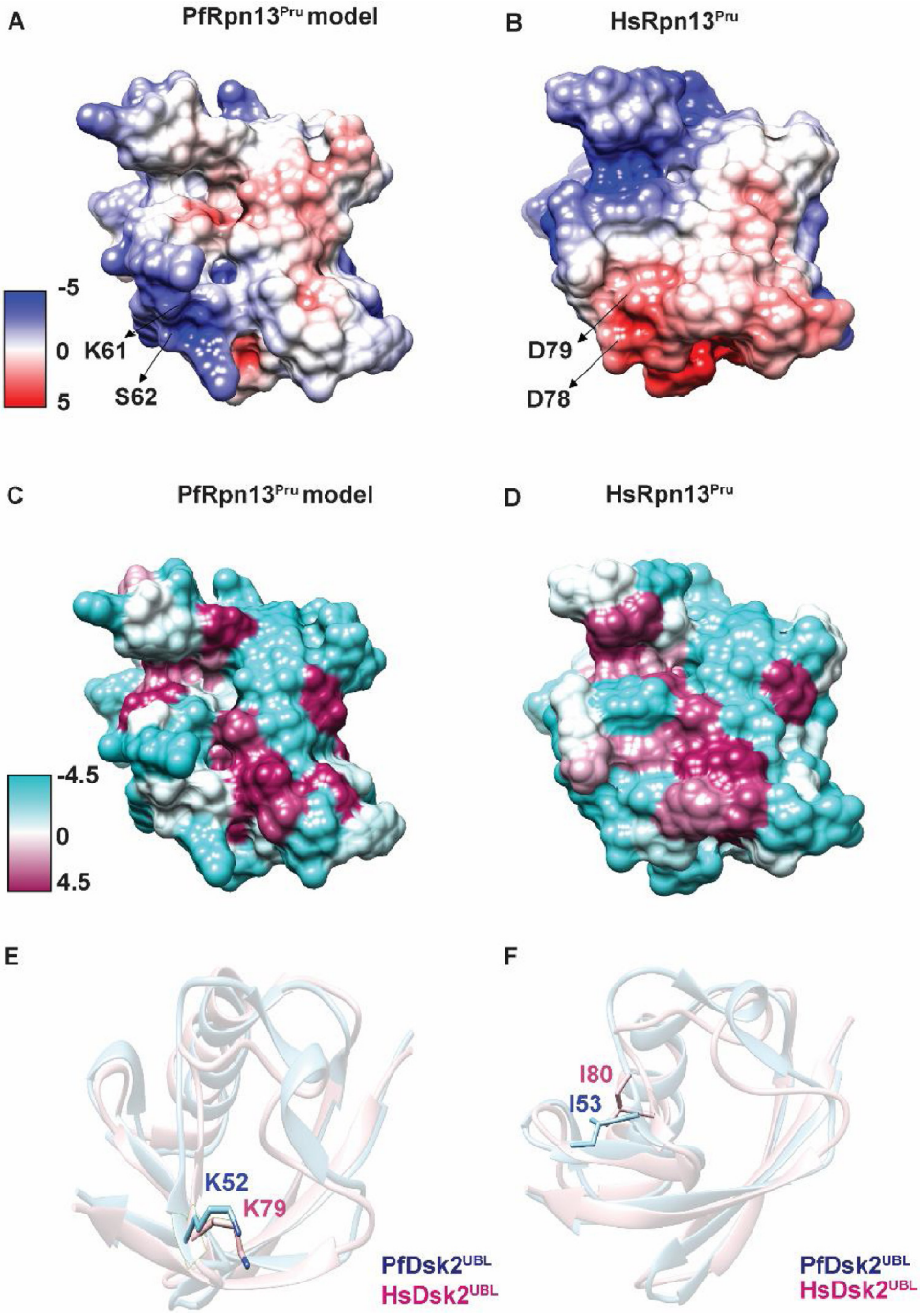

Fig. 5. APBS-derived surface electrostatics of (A) Modeled PfRpn13^{Pru} and (B) HsRpn13^{Pru}.The electrostatic comparison shows a more negative surface on HsRpn13^{Pru} due to presence of acidic residues Asp78 and Asp79 which are substituted with Lys61 and Ser62 on PfRpn13^{Pru}. The color scale is in units of kT/e ranging from −5 (red) to + 5 (blue). (C) Hydrophobic surface representation of modeled PfRpn13^{Pru} and (D) HsRpn13^{Pru}. Hydrophobic surface is represented by using the Kyle-Doolittle scale in the range of −4.5 to +4.5, with cyan for most hydrophilic to maroon for most hydrophobic residues. (E) Comparison of side chain orientation of residue Lys52 in PfDsk2^{UBL} (sky blue) and Lys79 in HsDsk2^{UBL} (pink) (F) Ile53 in PfDsk2^{UBL} and Ile80 in HsDsk2^{UBL} (pink).

tag itself. Therefore, it was not possible to conclude for the preference of UBL for UIM motifs. In humans Dsk2^{UBL} have a higher affinity for UIM1 due to additional contacts via longer helix as compared to UIM2.

4. Discussion

The role of the proteasome machinery in *Plasmodium falciparum* has garnered great attention since the development of proteasome inhibitors targeting the parasite [54–56]. The functions of shuttle proteins and the proteasome receptors associated with the proteasome have been putatively identified by bioinformatic approaches [24]. A recent protein-protein interaction study using yeast two hybrid assay has led to the identification of the interaction of a crucial virulence factor ETRAMP, with the shuttle protein Dsk2 [9]. This indicates that although our knowledge of parasite shuttle proteins is limited, it does potentially bear importance in the regulation of proteins related to parasite pathogenicity. Barring the proteasome however, there is very little information as to how protein turnover is regulated in parasites. One possible reason is that the fundamental mechanisms underlying the communication of turnover pathways with the proteasome remains unclear. In this study, we have performed a structural analysis of the UBL domain of the shuttle protein PfDsk2 and assessed the affinity of its binding to proteasomal receptors.

Prior to analyzing the interaction of the shuttle protein with the proteasome receptor, we have determined how the unbound structure of the UBL domain of the shuttle protein Dsk2 differs from its human ortholog. The UBL domain plays a key role in interaction with the proteasome receptors, Rpn10 and Rpn13 [14,57]. Subsequently, we have compared the binding site of the proteasome receptor on the UBL domain with the human ortholog and identified that the area of the

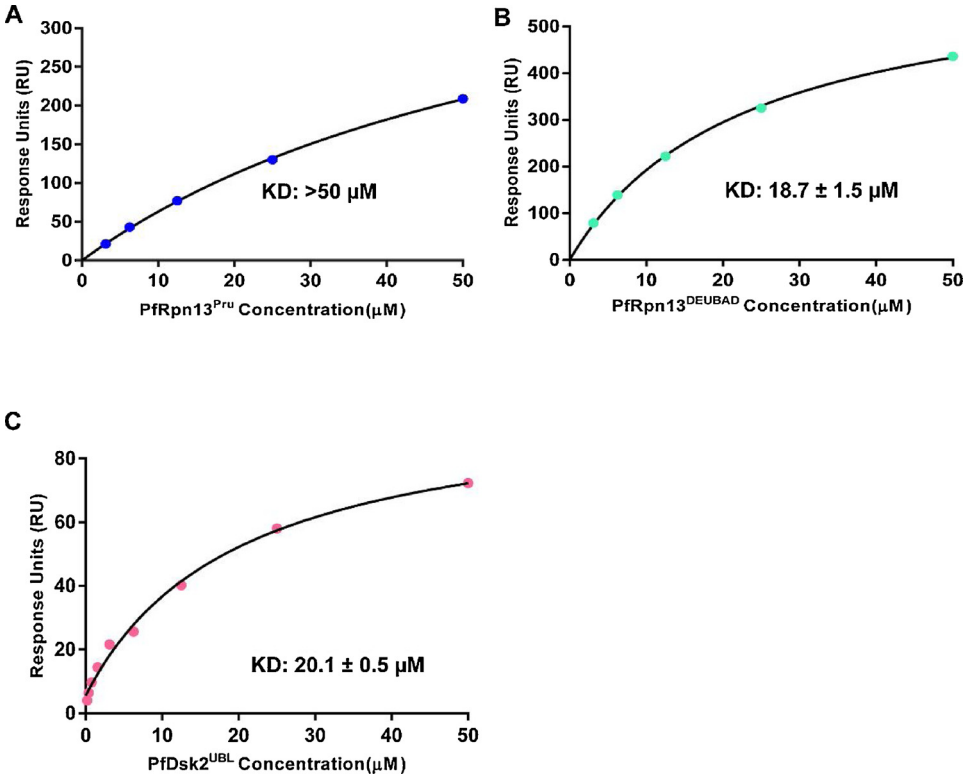

Fig. 6. Surface Plasmon resonance (SPR) assay characterizing binding of PfRpn13 and PfRpn10 domains with PfDsk2^{UBL}. (A) PfRpn13^{Pru} (3.125, 6.25, 12.5, 25 and 50 μM) over immobilized PfDsk2^{UBL}. (B) PfRpn13^{DEUBAD} (3.125, 6.25, 12.5, 25 and 50 μM) over immobilized PfDsk2^{UBL}. (C) PfDsk2^{UBL} (0.19, 0.39, 0.78, 1.56, 3.12, 6.25, 12.5, 25 and 50 μM) injected over immobilized PfRpn10^{UIM2}. The presented result is the representation of one of two independent replicates. The KD value with the standard deviation is shown.

binding interface as well as the solvent exposed residues are conserved. However, a few unique features were observed for PfDsk2^{UBL}. The first is the substitution of Ala77 in humans, known to be responsible for interaction with Rpn13^{Pru}, with Lys50 in *Plasmodium*. The second distinct feature is the substitution of Ser76 in place of Lys103, which plays a major role in forming the salt bridges with the acidic residues in Rpn10^{UIMs} motifs. These interactions, however, do not result in a loss or weakening of binding, as Dsk2^{UBL} shows binding with the corresponding proteasome receptors Rpn13^{Pru} and Rpn10^{UIM}. The third important feature is the substitution of Leu96 and Val98 with Asp69 and Met71 respectively at the second binding site, which create a less hydrophobic binding surface on PfDsk2^{UBL}. Also, the orientation of the side chains of Lys52 and Ile53 was distinct from HsDsk2^{UBL}, which could provide distant and additional contacts with PfRpn13^{Pru}. These two amino acids are known to mediate a salt bridge and hydrophobic interaction, respectively, bringing β4 of UBL in proximity to Rpn13^{Pru}. Future mechanistic studies of the shuttle proteins with the proteasome receptors would help identify the residues responsible for additional contacts and validate this possibility. Lastly, a striking feature was the completely opposite electrostatic surface of the α-helix which resembled non-shuttle UBL-containing proteins such as HsHOIL^{UBL}. These proteins do not function as shuttle proteins; however, HsHOIL interacts with other partners and plays a crucial role in other cellular functions, indicating the probability of *Plasmodium* Dsk2 performing additional functions.

The binding of PfRpn13^{DEUBAD} with PfDsk2^{UBL} is a unique feature observed in plasmodia. UCHL5, which is known to interact with HsRpn13^{DEUBAD} in human is not present in *Plasmodium* [50,58]. Nevertheless, few of the residues responsible for interaction with UCHL5 are conserved in PfRpn13^{DEUBAD}. This could hold the possibility of another deubiquitinating enzyme fulfilling the role of UCHL5 in plasmodia. One may assume that PfDsk2 itself could moonlight as a deubiquitinating enzyme but however, the residues responsible for deubiquitination activity are absent. Thus, the positive interaction with PfDsk2^{UBL} demonstrates the possibility of PfDsk2 working in cooperation with a deubiquitinating enzyme. Coupled with its HOIL-like negative binding surface, PfDsk2 merits a proteome-wide study to understand the extent of its ancillary activities.

The other receptor PfRpn10 showed UIM motifs that possess consensus sequences which are quite conserved in plasmodia. However, one of the main distinguishing features was the presence of Glu265 instead of Tyr289 in the UIM2. The importance of this residue in the interaction with human ortholog Dsk2 is not illustrated, but it plays a crucial role in the interaction with ubiquitin and HsRad23. The binding affinity of PfRpn10^{UIM2} with PfRad23^{UBL}, was found to be similar, however, to HsRad23^{UBL} making it inconclusive about the role of this substitution.

In conclusion, this study provides the first atomic resolution structure of the proteasome binding domain of a shuttle protein from apicomplexan parasites, along with how it relates to and differs from its human counterpart. Through binding studies, we have also theorized on how the structural features of PfDsk2^{UBL} may contribute to the affinity of binding with cognate receptors on the proteasome. The role of plasmodial shuttle proteins in degradation is one of their aspects which we have studied here, with other roles in eukaryotes being related to cell cycle and repair mechanism [20,22]. In yeast, the shuttle factors are not critical for survival, but in mice, LOF mutants of shuttle factors rarely survive till adulthood [19]. Broadly, this points towards the role of these proteins in supplementary functions which still need to be explored in *Plasmodium falciparum*. The shuttle protein PfDsk2 is known to interact with ETRAMP-5, a key protein family responsible for pathogenicity and virulence in parasite. However, whether the interaction leads to the subsequent degradation of this protein is inconclusive [9]. We hypothesize that if this interaction is hampered then it could subsequently lead to cellular stress in the parasite via accumulation of the misfolded proteins and this would disturb the protein homoeostasis in parasite. Building upon our present work, it could be possible to determine how PfDsk2 and PfRad23 recognize substrates, mediate their transport and facilitate their degradation through interaction with the proteasomal receptors. Subsequently, this could pave the way towards finding the role of plasmodial shuttle proteins as potential novel drug targets, especially given the current emergence of resistance against

anti-malaria drugs.

Accession number

Coordinates and structure factors have been deposited in the Protein Data Bank with accession number 6JL3.

Funding

This work was supported by Inspire Fellowship from Department of Science and Technology (DST), IndiaDST/INSPIRE/04/2014/000803. I.G. supported by Shyama Prasad Mukherjee Fellowship from Council of Scientific and Industrial Research (CSIR), India. S.K. supported by INSPIRE Fellowship from Department of Science and Technology (DST), India.

CRediT authorship contribution statement

Ishita Gupta: Conceptualization, Methodology, Validation, Investigation, Writing - original draft, Project administration. **Sameena Khan:** Conceptualization, Resources, Writing - review & editing, Supervision, Project administration, Funding acquisition.

Declaration of Competing Interest

The authors declare there is no conflict of interest with this work.

Acknowledgements

We thank. Dr. Akshay Kumar Ganguly for discussion and critical reading of manuscript. We thank Dr. Abhishek Jamwal for assistance in structure determination. Crystal diffraction data was collected at ESRF Beamline 23-1. We thank Dr. Nishant Kumar Varshney and beamline scientist at ESRF Beamline for data collection assistance.

Appendix A. Supplementary data

Supplementary material related to this article can be found, in the online version, at doi:https://doi.org/10.1016/j.molbiopara.2020.111266.

References

[1] Y. Saeki, Ubiquitin recognition by the proteasome, J. Biochem. 161 (2017) 113–124.
[2] V. Su, A.F. Lau, Ubiquitin-like and ubiquitin-associated domain proteins: significance in proteasomal degradation, Cell. Mol. Life Sci. 66 (2009) 2819–2833.
[3] P. Horrocks, C.I. Newbold, Intraerythrocytic polyubiquitin expression in Plasmodium falciparum is subjected to developmental and heat-hock control, Mol. Biochem. Parasitol. 105 (2000) 115–125.
[4] N. Ponts, A. Saraf, D.-W.D. Chung, A. Harris, J. Prudhomme, M.P. Washburn, L. Florens, K.G. Le Roch, Unraveling the ubiquitome of the human malaria parasite, J. Biol. Chem. 286 (2011) 40320–40330.
[5] G. Kleiger, T. Mayor, Perilous journey: a tour of the ubiquitin–proteasome system, Trends Cell Biol. 24 (2014) 352–359.
[6] A. Varshavsky, Regulated protein degradation, Trends Biochem. Sci. 30 (2005) 283–286.
[7] E. Itakura, E. Zavodszky, S. Shao, M.L. Wohlever, R.J. Keenan, R.S. Hegde, Ubiquilins chaperone and triage mitochondrial membrane proteins for degradation, Mol. Cell 63 (2016) 21–33.
[8] R. Suzuki, H. Kawahara, UBQLN4 recognizes mislocalized transmembrane domain proteins and targets these to proteasomal degradation, EMBO Rep. 17 (2016) 842–857.
[9] D.J. LaCount, M. Vignali, R. Chettier, A. Phansalkar, R. Bell, J.R. Hesselberth, L.W. Schoenfeld, I. Ota, S. Sahasrabudhe, C. Kurschner, A protein interaction network of the malaria parasite Plasmodium falciparum, Nature 438 (2005) 103.
[10] T. Spielmann, D.J. Fergusen, H.-P. Beck, Etramps, a new Plasmodium falciparum gene family coding for developmentally regulated and highly charged membrane proteins located at the parasite–host cell interface, Mol. Biol. Cell 14 (2003) 1529–1544.
[11] M. Vignali, A. McKinlay, D.J. LaCount, R. Chettier, R. Bell, S. Sahasrabudhe, R.E. Hughes, S. Fields, Interaction of an atypical Plasmodium falciparum ETRAMP with human apolipoproteins, Malar. J. 7 (2008) 211.
[12] J. Miller, C. Gordon, The regulation of proteasome degradation by multi-ubiquitin chain binding proteins, FEBS Lett. 579 (2005) 3224–3230.
[13] R. Hjerpe, J.S. Bett, M.J. Keuss, A. Solovyova, T.G. McWilliams, C. Johnson, I. Sahu, J. Varghese, N. Wood, M. Wightman, UBQLN2 mediates autophagy-independent protein aggregate clearance by the proteasome, Cell 166 (2016) 935–949.
[14] K. Husnjak, S. Elsasser, N. Zhang, X. Chen, L. Randles, Y. Shi, K. Hofmann, K.J. Walters, D. Finley, I. Dikic, Proteasome subunit Rpn13 is a novel ubiquitin receptor, Nature 453 (2008) 481.
[15] Y. Shi, X. Chen, S. Elsasser, B.B. Stocks, G. Tian, B.-H. Lee, Y. Shi, N. Zhang, S.A. de Poot, F. Tuebing, Rpn1 provides adjacent receptor sites for substrate binding and deubiquitination by the proteasome, Science 351 (2016) aad9421.
[16] K.J. Walters, M.F. Kleijnen, A.M. Goh, G. Wagner, P.M. Howley, Structural studies of the interaction between ubiquitin family proteins and proteasome subunit S5a, Biochemistry 41 (2002) 1767–1777.
[17] J.M. Ng, W. Vermeulen, G.T. van der Horst, S. Bergink, K. Sugasawa, H. Vrieling, J.H. Hoeijmakers, A novel regulation mechanism of DNA repair by damage-induced and RAD23-dependent stabilization of xeroderma pigmentosum group C protein, Genes Dev. 17 (2003) 1630–1645.
[18] S. Biggins, I. Ivanovska, M.D. Rose, Yeast ubiquitin-like genes are involved in duplication of the microtubule organizing center, J. Cell Biol. 133 (1996) 1331–1346.
[19] L. Chen, K. Madura, Rad23 promotes the targeting of proteolytic substrates to the proteasome, Mol. Cell. Biol. 22 (2002) 4902–4913.
[20] Z. Xie, S. Liu, Y. Zhang, Z. Wang, Roles of Rad23 protein in yeast nucleotide excision repair, Nucleic Acids Res. 32 (2004) 5981–5990.
[21] G.H. Baek, I. Kim, H. Rao, The Cdc48 ATPase modulates the interaction between two proteolytic factors Ufd2 and Rad23, Proc. Natl. Acad. Sci. 108 (2011) 13558–13563.
[22] L.A. Díaz-Martínez, Y. Kang, K.J. Walters, D.J. Clarke, Yeast UBL-UBA proteins have partially redundant functions in cell cycle control, Cell Div. 1 (2006) 28.
[23] L. Chen, K. Madura, Evidence for distinct functions for human DNA repair factors hHR23A and hHR23B, FEBS Lett. 580 (2006) 3401–3408.
[24] L. Wang, C. Delahunty, K. Fritz-Wolf, S. Rahlfs, J.H. Prieto, J.R. Yates, K. Becker, Characterization of the 26S proteasome network in Plasmodium falciparum, Sci. Rep. 5 (2015) 17818.
[25] S. Jantrapirom, L.L. Piccolo, H. Yoshida, M. Yamaguchi, A new Drosophila model of Ubiquilin knockdown shows the effect of impaired proteostasis on locomotive and learning abilities, Exp. Cell Res. 362 (2018) 461–471.
[26] D. Lambertson, L. Chen, K. Madura, Pleiotropic defects caused by loss of the proteasome-interacting factors Rad23 and Rpn10 of Saccharomyces cerevisiae, Genetics 153 (1999) 69–79.
[27] H. Rao, A. Sastry, Recognition of specific ubiquitin conjugates is important for the proteolytic functions of the ubiquitin-associated domain proteins Dsk2 and Rad23, J. Biol. Chem. 277 (2002) 11691–11695.
[28] A.M. Whiteley, M.A. Prado, I. Peng, A.R. Abbas, B. Haley, J.A. Paulo, M. Reichelt, A. Katakam, M. Sagolla, Z. Modrusan, Ubiquilin1 promotes antigen-receptor mediated proliferation by eliminating mislocalized mitochondrial proteins, elife 6 (2017) e26435.
[29] S. Delagenière, P. Brenchereau, L. Launer, A.W. Ashton, R. Leal, S. Veyrier, J. Gabadinho, E.J. Gordon, S.D. Jones, K.E. Levik, ISPyB: an information management system for synchrotron macromolecular crystallography, Bioinformatics 27 (2011) 3186–3192.
[30] J. Gabadinho, A. Beteva, M. Guijarro, V. Rey-Bakaikoa, D. Spruce, M.W. Bowler, S. Brockhauser, D. Flot, E.J. Gordon, D.R. Hall, MxCuBE: a synchrotron beamline control environment customized for macromolecular crystallography experiments, J. Synchrotron Radiat. 17 (2010) 700–707.
[31] D. Nurizzo, T. Mairs, M. Guijarro, V. Rey, J. Meyer, P. Fajardo, J. Chavanne, J.-C. Biasci, S. McSweeney, E. Mitchell, The ID23-1 structural biology beamline at the ESRF, J. Synchrotron Radiat. 13 (2006) 227–238.
[32] W. Kabsch, Integration, scaling, space-group assignment and post-refinement, Acta Crystallogr. D Biol. Crystallogr. 66 (2010) 133–144.
[33] P.R. Evans, G.N. Murshudov, How good are my data and what is the resolution? Acta Crystallogr. D Biol. Crystallogr. 69 (2013) 1204–1214.
[34] P.D. Adams, P.V. Afonine, G. Bunkóczi, V.B. Chen, I.W. Davis, N. Echols, J.J. Headd, L.-W. Hung, G.J. Kapral, R.W. Grosse-Kunstleve, PHENIX: a comprehensive Python-based system for macromolecular structure solution, Acta Crystallogr. D Biol. Crystallogr. 66 (2010) 213–221.
[35] E.D. Lowe, Ni. Hasan, J.-F. Trempe, L. Fonso, M.E. Noble, J.A. Endicott, L.N. Johnson, N.R. Brown, Structures of the Dsk2 UBL and UBA domains and their complex, Acta Crystallogr. D Biol. Crystallogr. 62 (2006) 177–188.
[36] P.V. Afonine, R.W. Grosse-Kunstleve, N. Echols, J.J. Headd, N.W. Moriarty, M. Mustyakimov, T.C. Terwilliger, A. Urzhumtsev, P.H. Zwart, P.D. Adams, Towards automated crystallographic structure refinement with phenix. Refine, Acta Crystallogr. D Biol. Crystallogr. 68 (2012) 352–367.
[37] P. Emsley, B. Lohkamp, W.G. Scott, K. Cowtan, Features and development of coot, Acta Crystallogr. D Biol. Crystallogr. 66 (2010) 486–501.
[38] W.L. DeLano, Pymol: An open-source molecular graphics tool, CCP4 Newslett. Protein Crystallogr. 40 (2002) 82–92.
[39] E.F. Pettersen, T.D. Goddard, C.C. Huang, G.S. Couch, D.M. Greenblatt, E.C. Meng, T.E. Ferrin, UCSF Chimera—a visualization system for exploratory research and analysis, J. Comput. Chem. 25 (2004) 1605–1612.
[40] E. Krissinel, K. Henrick, Inference of macromolecular assemblies from crystalline state, J. Mol. Biol. 372 (2007) 774–797.
[41] A. Waterhouse, M. Bertoni, S. Bienert, G. Studer, G. Tauriello, R. Gumienny, F.T. Heer, T.A.P. de Beer, C. Rempfer, L. Bordoli, R. Lepore, T. Schwede, SWISS-MODEL: homology modelling of protein structures and complexes, Nucleic Acids

Res. 46 (2018) W296–W303.
[42] Aneerban Bhattacharya, Roberto Tejero, Gaetano T. Montelione, Evaluating protein structures determined by structural genomics consortia, Proteins Struct. Funct. Bioinform. 66 (2007) 778–795.
[43] D.J. Oshannessy, M. Brighamburke, K.K. Soneson, P. Hensley, I. Brooks, Determination of rate and equilibrium binding constants for macromolecular interactions using surface plasmon resonance: use of nonlinear least squares analysis methods, Anal. Biochem. 212 (1993) 457–468.
[44] Ralf W. Glaser, Antigen-antibody binding and mass transport by convection and diffusion to a surface: a two-dimensional computer model of binding and dissociation kinetics, Anal. Biochem. 213 (1993) 152–161.
[45] X. Robert, P. Gouet, Deciphering key features in protein structures with the new ENDscript server, Nucleic Acids Res. 42 (W1) (2014) W320–W324.
[46] X. Chen, D.L. Ebelle, B.J. Wright, V. Sridharan, E. Hooper, K.J. Walters, Structure of hRpn10 bound to UBQLN2 UBL illustrates basis for complementarity between shuttle factors and substrates at the proteasome, J. Mol. Biol. 431 (2019) 939–955.
[47] Hirokazu Yagi, Kazuhiro Ishimoto, Takeshi Hiromoto, Hiroaki Fujita, Tsunehiro Mizushima, Yoshinori Uekusa, Maho Yagi-Utsumi, et al., A non-canonical UBA–UBL interaction forms the linear-ubiquitin-chain assembly complex, EMBO Rep. 13 (2012) 462–468.
[48] X. Chen, L. Randles, K. Shi, S.G. Tarasov, H. Aihara, K.J. Walters, Structures of Rpn1 T1: Rad23 and hRpn13: hPLIC2 reveal distinct binding mechanisms between substrate receptors and shuttle factors of the proteasome, Structure 24 (2016) 1257–1270.
[49] Q. Wang, P. Young, K.J. Walters, Structure of S5a bound to monoubiquitin provides a model for polyubiquitin recognition, J. Mol. Biol. 348 (2005) 727–739.
[50] D.D. Sahtoe, W.J. van Dijk, F. El Oualid, R. Ekkebus, H. Ovaa, T.K. Sixma, Mechanism of UCH-L5 activation and inhibition by DEUBAD domains in RPN13 and INO80G, Mol. Cell 57 (2015) 887–900.
[51] P. Schreiner, X. Chen, K. Husnjak, L. Randles, N. Zhang, S. Elsasser, D. Finley, I. Dikic, K.J. Walters, M. Groll, Ubiquitin docking at the proteasome through a novel pleckstrin-homology domain interaction, Nature 453 (2008) 548.
[53] T.D. Mueller, J. Feigon, Structural determinants for the binding of ubiquitin-like domains to the proteasome, EMBO J. 22 (2003) 4634–4645.
[54] K.M. Krishnan, K.C. Williamson, The proteasome as a target to combat malaria: hits and misses, Transl. Res. 198 (2018) 40–47.
[55] S. Crunkhorn, Antimalarials: novel proteasome inhibitor combats malaria, Nat. Rev. Drug Discov. 15 (2016) 232.
[56] B.H. Stokes, E. Yoo, J.M. Murithi, M.R. Luth, P. Afanasyev, P.C. da Fonseca, E.A. Winzeler, C.L. Ng, M. Bogyo, D.A. Fidock, Covalent Plasmodium falciparum-selective proteasome inhibitors exhibit a low propensity for generating resistance in vitro and synergize with multiple antimalarial agents, PLoS Pathog. 15 (2019) e1007722.
[57] S. Elsasser, D. Chandler-Militello, B. Müller, J. Hanna, D. Finley, Rad23 and Rpn10 serve as alternative ubiquitin receptors for the proteasome, J. Biol. Chem. 279 (2004) 26817–26822.
[58] R.T. VanderLinden, C.W. Hemmis, B. Schmitt, A. Ndoja, F.G. Whitby, H. Robinson, R.E. Cohen, T. Yao, C.P. Hill, Structural basis for the activation and inhibition of the UCH37 deubiquitylase, Mol. Cell 57 (2015) 901–911.